JACS
JOURNAL OF THE AMERICAN CHEMICAL SOCIETY
Article
pubs.acs.org/JACS

Reconciling the Roles of Kinetic and Thermodynamic Factors in Membrane–Protein Insertion

James C. Gumbart,[†] Ivan Teo,[‡] Benoît Roux,*[,§] and Klaus Schulten*[,‡]

[†]School of Physics, Georgia Institute of Technology, Atlanta, Georgia 30363, United States
[‡]Beckman Institute and Department of Physics, University of Illinois at Urbana–Champaign, Urbana, Illinois 61801, United States
[§]Department of Biochemistry and Molecular Biology and Gordon Center for Integrative Science, The University of Chicago, Chicago, Illinois 60637, United States

Supporting Information

ABSTRACT: For the vast majority of membrane proteins, insertion into a membrane is not direct, but rather is catalyzed by a protein-conducting channel, the translocon. This channel provides a lateral exit into the bilayer while simultaneously offering a pathway into the aqueous lumen. The determinants of a nascent protein's choice between these two pathways are not comprehensively understood, although both energetic and kinetic factors have been observed. To elucidate the specific roles of some of these factors, we have carried out extensive all-atom molecular dynamics simulations of different nascent transmembrane segments embedded in a ribosome-bound bacterial translocon, SecY. Simulations on the μs time scale reveal a spontaneous motion of the substrate segment into the membrane or back into the channel, depending on its hydrophobicity. Potential of mean force (PMF) calculations confirm that the observed motion is the result of local free-energy differences between channel and membrane. Based on these and other PMFs, the time-dependent probability of membrane insertion is determined and is shown to mimic a two-state partition scheme with an apparent free energy that is compressed relative to the molecular-level PMFs. It is concluded that insertion kinetics underlies the experimentally observed thermodynamic partitioning process.

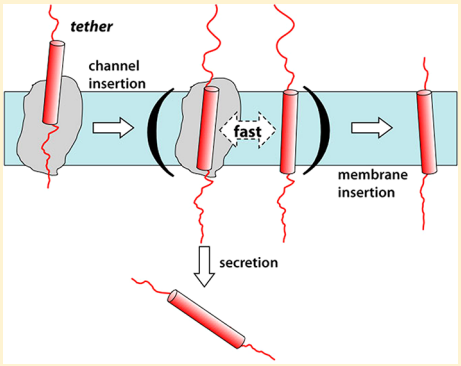

INTRODUCTION

Synthesis and insertion of membrane proteins into a lipid bilayer is a fundamental biophysical process for which many aspects are not yet understood. Insertion occurs co-translationally via a highly conserved and specialized membrane channel, the so-called SecY translocon, which possesses a lateral gate for exit of transmembrane (TM) segments into the lipid bilayer.[1−3] This SecY channel, in addition to providing a pathway into the membrane, also permits water-soluble proteins or periplasmic domains of membrane proteins to be secreted across the bilayer, thus acting as a switching point for protein localization.

The energetics of the membrane-insertion process have been characterized by the beautiful experimental work of von Heijne and colleagues.[4,5] However, their results have led to two currently unresolved issues that present a great puzzle to researchers in the field. The first concerns the magnitude of the apparent transfer free energy, the so-called "biological hydrophobic scale".[4] Surprisingly, the scale was found to span a narrow range of only 3−4 kcal/mol for all 20 amino acids, in stark contrast to considerations based on the physical chemistry of hydration, as well as computational predictions.[6] The second outstanding and unresolved issue concerns the actual role played by non-equilibrium kinetics in the membrane-insertion process. Peptide translation by the ribosome, which is driven at a rate of ∼10−20 residues/s through peptide synthesis,[7] is an irreversible non-equilibrium process. However, whether peptide transfer from the translocon to the membrane occurring in the later stages is primarily governed by equilibrium or non-equilibrium events is unknown.[8]

The striking similarity of the measured biological hydrophobic scale with a two-state partition scheme[4,5,9] has led many to postulate that insertion into the membrane occurring in the later stage must reflect a purely thermodynamic equilibrium process, making dynamics of the process largely irrelevant to understanding it. Nevertheless, the molecular character of these two putative states is not known, and it is unlikely that they would correspond to fully secreted or fully membrane-inserted helix configurations.[8,10,11] An alternative proposal attributing more importance to non-equilibrium aspects stipulates that modulation of the channel's gating kinetics by the nascent peptide is the dominant factor controlling whether a peptide ends up being inserted into the membrane or secreted into the cytoplasm, although membrane-peptide interactions still play a role.[12] In support of this view, simulation studies show aspects of opening of the translocon by the signal anchor (SA), itself a TM segment, and factors controlling its orientation.[13] However, the similarities of scales determined for different

Received: November 1, 2012
Published: January 8, 2013

   dx.doi.org/10.1021/ja310777k | J. Am. Chem. Soc. 2013, 135, 2291−2297

membranes, including the bacterial cytoplasmic membrane[14] and the mitochondrial inner membrane,[15] as well as the temperature dependence of insertion[16] are indicative of additional factors that are not channel-specific. Despite the great progress, fundamental questions remain about the respective roles played by energetic and kinetic effects and how non-equilibrium effects come into play during the membrane-insertion process.

To answer these questions, we relied on multiple computational approaches, including μs atomic-scale molecular dynamics (MD) simulations on Anton,[17] umbrella sampling (US) potential of mean force (PMF) computations, and stochastic simulation of a diffusion–elongation model describing the process of membrane insertion over a time scale of seconds. The results lead to the formulation of a novel hypothesis that connects the translation rate with insertion, mediated via the progressive elongation of the nascent chain length, in agreement with previous experiments. By effectively coupling two widely disparate time scales—a very short one governing local motion of the TM segment in the translocon and a very long one dictated by the rates of translation and translocation—it is found that an apparent two-state thermodynamic partition scheme consistent with the biological hydrophobic scale arises actually from a non-equilibrium diffusion–elongation process.

METHODS

Construction of the simulated ribosome–translocon system began with the structure from Frauenfeld et al.,[18] which contains the full ribosome bound to SecYE with a nascent chain and its SA present (PDB identifiers 3J00/3J01). Because only dynamics near the channel and membrane are of interest in the current study, the ribosome was truncated such that only atoms within 20 Å of the channel were kept, ribosome atoms near the truncation boundary being harmonically restrained. Additionally, the majority of the nascent chain was removed from the system, leaving only the SA. The channel was embedded in a 200-lipid mixed 75%/25% POPE/POPG membrane, which mimics the bacterial membrane.[19] The resulting system contains approximately 120 000 atoms and is shown in Figure S1 (Supporting Information). All figures were made using VMD.[20]

NAMD Simulations. All equilibration and US simulations were carried out using NAMD[21] along with the CHARMM22/CMAP[22,23] force field for proteins and CHARMM36 for lipids.[24] A multiple time-stepping algorithm was employed with a 2-fs integration time step and short-range and long-range non-bonded interactions (separated by a cutoff at 12 Å) evaluated every 1 and 3 time steps, respectively. Long-range electrostatics were determined using the particle-mesh Ewald method. After equilibration at a constant pressure of 1 atm, the volume was held constant. Unless otherwise stated, all simulations were run at a constant temperature of 323 K.

Long-Time Simulations. Long-time simulations on Anton used the same system, force field, and multiple-time-stepping procedure as those run using NAMD. Constant volume and temperature were maintained using the Berendsen coupling scheme. Although an isotropic pressure control, in which the membrane area can fluctuate, is preferred for CHARMM36 lipids,[24] the repulsion between neighboring ribosome images may unnaturally influence the unit-cell area. Comparison of the excluded area as a function of z for the membrane between the fully open and fully closed states of SecYE reveals that they are nearly identical (see Figure S2).

Long-range electrostatics were calculated using the k-Gaussian Split Ewald method on a 64×64×64 grid. The cutoff was determined independently for each simulation, but typically was around 13 Å. For simulations investigating the motion of a substrate helix located at the lateral gate, i.e., those illustrated in Figure 2, an elevated temperature of 353 K was employed to enhance the likelihood of observing helix movement on the μs time scale; all other simulations on Anton were carried out at 323 K. Temperatures of 353–490 K have previously been validated for peptide–membrane partitioning studies and were found to not significantly affect the systems' thermodynamic properties.[25] The total time for all Anton simulations is ∼30 μs.

PMF Calculations. The PMFs shown in Figure 3B were calculated with US simulations,[26,27] using the colvars module of NAMD.[28] For each of the three substrate helices examined, i.e., the SA, polyLeu, and polyGln helices, 26 windows typically spaced 1 Å apart, beginning at the center of SecY and ending in the membrane, were used. The final PMFs were determined by unbiasing the histograms, shown in Figure S13, using the weighted histogram analysis method (WHAM).[29] The net simulation time for each helix is 250 ns, giving 750 ns in total.

Diffusion–Elongation Calculations. Calculations of translocation probabilities were carried out in Matlab. The algorithms developed involved integration of the Boltzmann distribution over 5000 irregular cells of a Voronoi tessellation outside of a predefined cutoff radius from the center of the SecY channel, up to 2000 Å. In order to verify that the system achieves equilibrium on a time scale much smaller than that of the translocation process, a more rigorous approach involving the solution of the Smoluchowski diffusion equation was used, and the results were compared to those from the Boltzmann simulation for an example case. In each simulation, the potential used was composed of a widening harmonic potential mimicking the effect of a lengthening polymer chain (see Figure 3B) and a linear fit of the radial PMF determined by all-atom US calculations. Simulations were run for up to 50 s with a time step falling in the range between 0.002 and 2 s. Details of the discretization scheme, simulation algorithms, and validation simulations can be found in the Supporting Information.

Parameters in the diffusion–elongation calculations were taken from multiple sources. The growth rate of the nascent chain is tied to the translation rate (for co-translational translocation), which is between 0.5 and 20 residues/s.[7,30,31] We estimated the lateral diffusion rate of the substrate helix from restrained US simulations,[32] finding it to fall in a range from 250 Å^2/μs in the channel to 1000 Å^2/μs in the membrane, in agreement with an experimental rate of 830 Å^2/μs.[33] The rate of translocation of the nascent chain through the channel has been determined in at least one case to be 1.6× the rate of translation, i.e., ∼4 s for 30 residues,[34] although this rate is sequence-dependent.[16,35] The rate of translocation affects the time available to the nascent chain in the channel to commit to the membrane-integrated or secreted pathways (see Figure 4). The channel radius, r_{cutoff}, is taken to be 12 Å based on the structure used (see Figure 3A), although a range of 10–15 Å is considered.

RESULTS

The simulations carried out in this study cover multiple functional aspects of the translocon SecY and the membrane insertion process. First, the dynamics of SecY, and its lateral gate in particular, in the presence or absence of different substrate helices embedded within are explored on the μs time scale. Next, the dynamics of a substrate helix at SecY's lateral gate are addressed. Finally, free-energy and finite-element calculations of complete membrane integration are presented.

Dynamics of SecY's Lateral Gate. It has been suggested previously that the opening and closing of SecY's lateral gate is controlled by the hydrophobicity of the nascent protein within the channel, with hydrophobic polypeptide segments inducing gate opening and hydrophilic ones gate closing.[12] To examine this suggestion, simulations ranging from 500 ns to 2 μs of a ribosome-bound SecY (see Figure S1) containing different nascent helices at its center, as well as none, were carried out. Specifically, a native SA, polyLeu, polySer, and polyGln were tested for different initial openings of SecY's lateral gate, including closed and partially or fully open gates, with the distance between the C_α atoms of residues Ser87 on SecY TM2b and Phe286 on TM7 monitored over time (see Figure

1). These residues were chosen as they were also used to monitor gate opening in cross-linking experiments under different translocation conditions.[36]

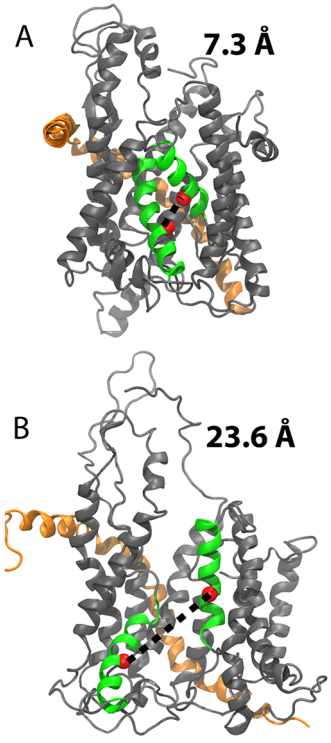

Figure 1. Lateral gate opening: SecYE shown in gray (SecY) and orange (SecE), with lateral gate helices TM2b and TM7 highlighted in green and residues Ser87 and Phe286 shown as red spheres. (A) Closed state of the gate (Ser87−Phe286 distance of 7.3 Å).[3] (B) Open state from a membrane-protein-insertion intermediate structure.[18]

For simulations beginning with a closed lateral gate (7−10 Å wide, Figure 1A), the gate opening did fluctuate, but no correlation between the magnitude of gate opening and hydrophobicity of the embedded helix was observed (see Figures S3 and S4). Similarly, no such correlation appeared when the gate was started in a partially open state (14 Å) nor in a fully open state (27 Å). In contrast, in all cases, the helix's contact with lipids was found to depend on its hydrophobicity, with the SA and polyLeu helices increasing their contact with lipids and the polySer and polyGln helices decreasing their contact (see Figure S5). The change in interaction area for hydrophobic segments results not from alterations to the lateral gate, but rather from incursion of lipid tails into the channel, shown in Figure S6. Thus, direct interaction between the substrate helix and lipids controls its position with respect to the channel center, rather than modulation of the gate by the helix.

Structures of SecY bound to different partners[37−39] displaying a partially open lateral gate have contributed to the hypothesis that partner binding can "pre-activate" the channel.[1] Electrophysiology experiments on ribosome−channel complexes have demonstrated that the channel remains permeable to ions and small molecules after removal of the nascent chain;[40−42] simulations on the 10-ns time scale have also shown that ribosome binding can subtly bias the closed channel toward an open state.[43] To further examine the role of ribosome binding on lateral gate opening, simulations of SecY with and without a ribosome bound were performed for 1.25 μs for both the closed channel and one at an intermediate gate opening (four simulations in total). As illustrated in Figure S3D, for both initial openings, the ribosome-bound SecY became more open laterally than the free SecY. For the closed SecY a slight increase in gate separation was observed with the ribosome bound; conversely, for the initially open SecY the gate began to close without a ribosome bound, supporting a role of channel-partner binding in inducing SecY to open partially. Differences in ion conductance for the ribosome-bound and free SecY could not be explicitly determined due to the limited frequency of coordinate output on Anton, although it is expected that the former is higher.[44]

TM Segment Behavior at the Lateral Gate. The structure of a nascent membrane-protein-insertion intermediate localizes the SA to the open lateral gate of SecY, at the boundary between channel and membrane.[18] However, from this structure alone, it cannot be concluded that a TM segment will move into the membrane spontaneously, as predicted by a thermodynamic partitioning model of membrane insertion.[9] Therefore, to explore the dynamics of the SA at the lateral gate, a system consisting of the membrane-bound SecYE along with a portion of the ribosome and the TM segment was constructed and simulated. Equilibrium simulations of 2.5 μs each were carried out on Anton at an elevated temperature of T = 353 K (see Methods) for the SA, as well as polyLeu and

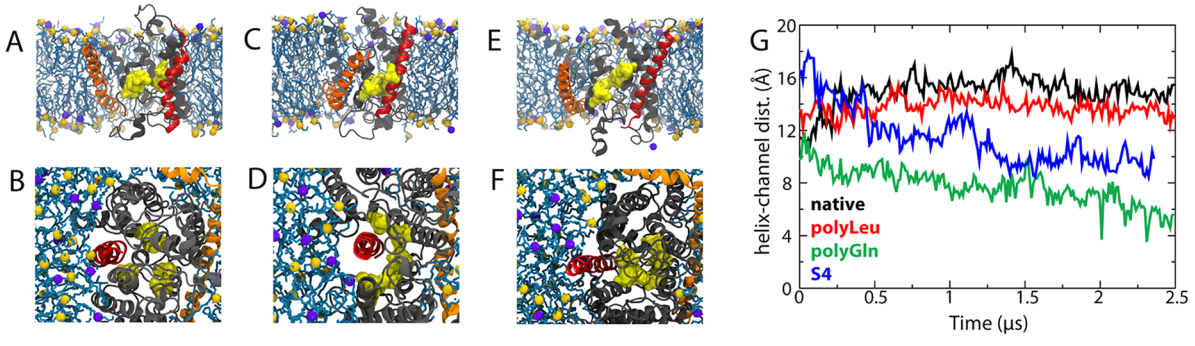

Figure 2. Spontaneous motion of a helix in SecY. SecYE (gray and orange, respectively) is shown in the membrane plane, cut perpendicularly to reveal the pore ring in yellow (A,C,E), and from the cytoplasmic side (B,D,F). The membrane is displayed as blue sticks with purple/yellow spheres for the phosphorus atoms. The substrate helix is shown in red. (A,B) Initial state (t = 0). (C,D) Final state (t = 2.5 μs) for polyGln. (E,F) Final state for polyLeu. (G) Plot of separation between the helix and the center of the SecY channel for four segments: SA (black), polyLeu (red), polyGln (green), and the S4 helix of KvAP (blue).

dx.doi.org/10.1021/ja310777k | J. Am. Chem. Soc. 2013, 135, 2291−2297

polyGln helices, in order to accelerate potential motions into or out of SecY. Finally, the KvAP S4 TM segment, which, when isolated, is just above the threshold for membrane insertion,[45] was also tested.

For the two hydrophobic TM segments, the SA and polyLeu helix, a gradual movement into the bilayer was observed. In both cases the helix moved 4−5 Å into the membrane; furthermore, SecY's lateral gate closed behind it (see Figure 2E,F). Additionally, the constrictive pore ring at the center of SecY closes, preventing return of the helix to the channel. Simulation of the SA at T = 323 K demonstrates the same motion as at 353 K, but to a lesser degree (see Figure S7). In contrast, the polyGln and S4 helices move 5−7 Å from the lateral gate region back into the center of SecY, with the pore ring opening wider to accommodate them, shown in Figure 2C,D and Figure S8. The interior of the channel is predominantly hydrophilic,[46,47] making it a significantly more favorable environment for the polyGln and S4 helices than the lateral gate and surrounding membrane. As above, the diffusion of the helix is found to correlate well with contact with lipid acyl tails, which wrap around the TM segments, bringing them into the membrane, while rejecting the hydrophilic segments. Thus, the motions of individual lipids provide for rapid sampling of the membrane environment without requiring full exit of the nascent helix from the channel.

Thermodynamics of TM Segment Exit from SecY. Although the previously described simulations of TM segment motion at the lateral gate are suggestive of a thermodynamic partitioning process, the observed behavior is nonetheless undersampled. To quantify this behavior, the PMF as a function of substrate helix distance from the channel's center was determined for the SA, polyLeu, and polyGln helices. Each PMF was calculated using approximately 350 ns of US simulations at 323 K. Because lipid diffusion occurs on a time scale of tens of nanoseconds,[48] in order to fully relax the membrane surrounding the helix, initial states for every fourth window (i.e., every 4 Å) were generated from 70-ns equilibrium simulations run on Anton.

The PMFs, shown in Figure 3, illustrate the free-energy cost, or gain, for a substrate helix moving from the lateral gate into the membrane or back into the channel. While the SA and polyLeu helices find the membrane more favorable than the channel by 1−2 and 4−5 kcal/mol, respectively, the polyGln helix favors the channel by over 10 kcal/mol. The decrease in free energy on going from SecY to membrane for the SA and polyLeu helices is likely the origin of the force measured experimentally for helices in the translocon.[49] Using the ΔG prediction server,[5] one obtains an apparent free-energy difference for the polyGln helix ΔG = 19 kcal/mol and for the polyLeu helix ΔG = −7.5 kcal/mol; the SA gives ΔG = −0.75 kcal/mol. Although the agreement in the ranking of the three tested segments is promising, it remains that the ΔG values from simulation, even when taken far from the channel, are distinct from the predicted values; the statistical error in the PMFs is at most ±0.5 kcal/mol (see Figure S9), which is insufficient to explain the discrepancy. However, the outcome of a two-state kinetic process is not expected to approach a simple equilibrium partition scheme unless there are multiple back-and-forth transitions between the two states. To wit, 10 transitions gives a standard error of ±16%, while about 100 transitions are required to come within at least 5% of the correct equilibrium probability. It is unlikely that a nascent polypeptide could sample the two separate environments a sufficient number of times to yield an apparent partition coefficient between them, particularly given the prohibitive entropic cost of returning to the narrow channel after reaching a distant point in the membrane.

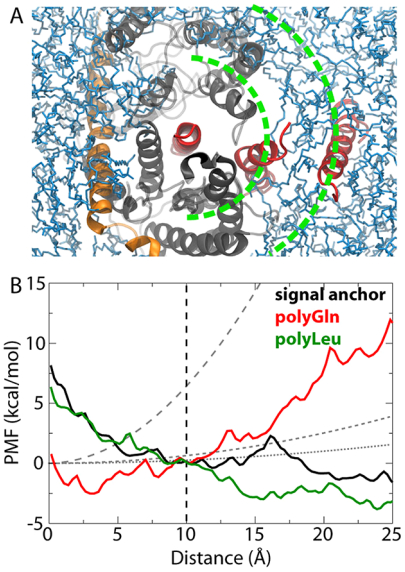

Figure 3. Potential of mean force for helix exit from SecY into the membrane. (A) SecY is shown from the cytoplasmic side in gray and orange with the membrane in blue. A substrate helix is shown in red at different positions along its exit, although only one helix was present at any given time. The green dotted lines are at r = 12 Å and r = 25 Å. (B) PMFs for the SA (black), polyLeu (green), and polyGln (red) helices as a function of distance from the channel center. The gray dashed lines show, in order of decreasing dash size, the restraining potential used in the diffusion calculations at times t = 1 s, 10 s, and 25 s.

Kinetics of TM Segment Exit from SecY. If the range of a nascent polypeptide were restricted instead of being completely free to move, then only a finite region in the immediate vicinity of the translocon would be sampled, with multiple possible returns to the channel center. Such a restriction could arise from, e.g., tethering to the remainder of the nascent chain, or interactions with the translocon or other chaperones in the membrane.[50] We have considered the first possibility, illustrated schematically in Figure 4, by solving for the 2D probability distribution of a substrate helix as a function of its radially dependent PMF with an added time-dependent restrictive potential arising from the elongation of the nascent chain. When a stop-transfer sequence, i.e., one that halts translocation, is in the channel, or during synthesis of a cytoplasmic domain, the nascent chain can accumulate outside the channel;[31] thus, we modeled the exposed, cytoplasmic portion of the nascent chain as a freely jointed chain, with the permitted lateral motion of the adjoining helix in the channel being roughly proportional to $\sqrt{N}$, where N is the number of residues that were added to the polypeptide by the ribosome. Integrating the 2D probability over the region outside the channel provides the probability of being in the membrane as a function of time.

Estimates for the parameters in the model were extracted from previous experiments or from simulations (see Methods), and their effect on insertion probability was determined. Decreasing the rate of translation, which ranges from 0.5 to 20 residue/s,[7,30,31] causes the TM segment to be retained near the channel longer and, thus, decreases the probability of insertion

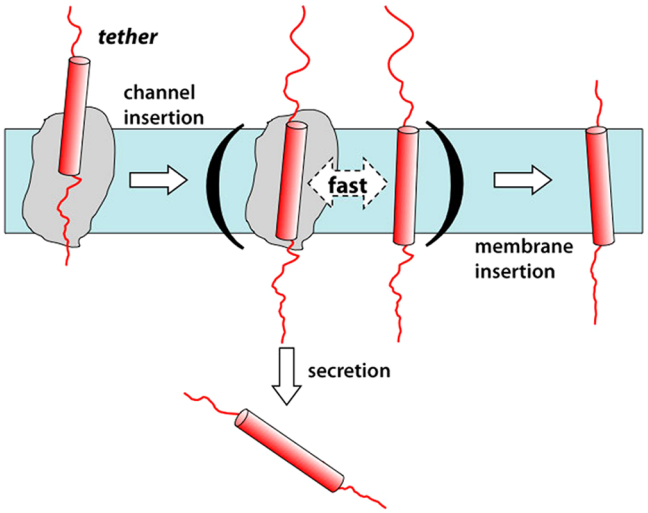

Figure 4. Schematic of TM segment insertion via the translocon. Upon entering SecY (gray), the putative TM segment (red) can equilibrate quickly in the immediate vicinity of the lateral gate, while still tethered to the ribosome (not shown for clarity). The unidirectional arrows indicate the irreversible processes (entry of nascent peptide into SecY and final expulsion into the solution or the membrane), whereas the double arrow indicates the local two-state kinetic process (between bold parentheses) responsible for the apparent thermodynamic partition coefficient. The commitment time is defined as the length of time the states in parentheses persist before an irreversible course into the membrane or the lumen is taken.

on the same time scale (see Figure S11A). However, if the rate of translation also alters the rate of translocation, such an effect may be muted; indeed, experimentally, when slowing translation from 0.5 to 0.25 residue/s, no change in insertion probability was observed.[30] Decreasing the rate of translocation, which is equivalent to increasing the commitment time, increases the membrane-insertion probability in our model, just as seen experimentally.[16] The effects of lateral gate opening and channel/membrane cutoff are also explored in Figure S11. Although the PMFs in Figure 3B are apparently quite noisy, the resulting probability curves are smooth, insensitive to the rugged energetic landscape, with insertion depending only on the overall slope.

To connect the time-dependent insertion probability to the biological hydrophobicity scale, simplified, linear PMFs were assumed in our kinetic model (see inset of Figure 5A and Figure S10), and the probability of membrane insertion as a function of time was calculated as shown in Figure 5A. Using the center of the channel and a location 15 Å away in the membrane as reference points, each PMF, and, thus, each insertion probability curve, can be assigned a value for ΔG(SecY→mem.); this value simply reflects the change in energy for going up (or down) the slope of each of the linear PMFs. Interestingly, the range of probabilities to insert into the membrane is broadest around ΔG(SecY→mem.) = 0; in other words, the difference in insertion probability between, e.g., −1.5 and 1.5 kcal/mol is much greater than that between 3 and 6 kcal/mol. This enhanced range explains the observed sensitivity of marginally hydrophobic helices to a myriad of factors. For example, slowing translocation through the channel enhances membrane integration for mildly hydrophobic TM segments.[16] Similarly, a greater carboxy-tail length succeeding the TM segment enhances integration, emphasizing the importance of

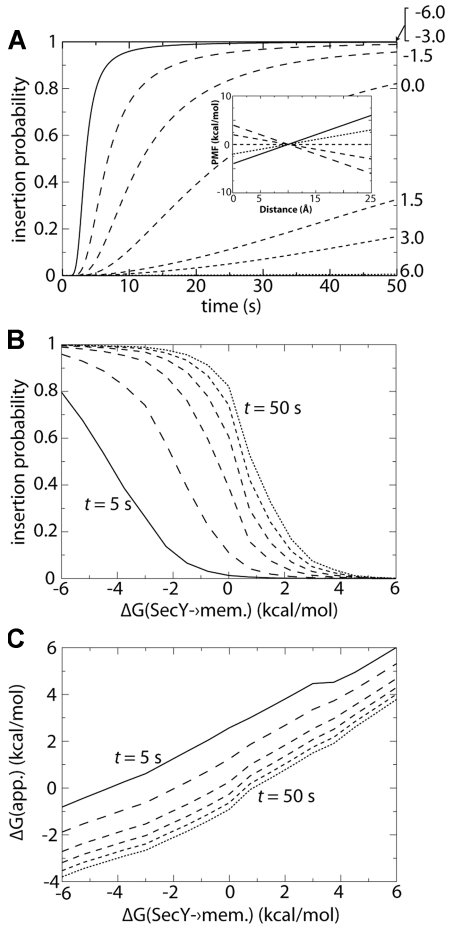

Figure 5. Membrane-insertion probability based on simplified PMFs. (A) Insertion probability as a function of time is plotted for linear PMFs of varying slope, shown in the inset plot and in Figure S10. The corresponding ΔG(SecY→mem.) values using a reference point 15 Å into the membrane are given to the right of each curve (a reference point of 25 Å is shown in Figure S12). (B) Insertion probability as a function of ΔG(SecY→mem.) for commitment times, from left to right, of t = 5, 10, 20, 30, 40, and 50 s. (C) Relationship between ΔG_{app} and ΔG(SecY→mem.) for the same commitment times as in part (B). ΔG_{app} is defined in the text.

holding the TM segment near the channel, rather than allowing it to translocate into the lumen.[30]

From the plot in Figure 5A, the insertion probability as a function of ΔG(SecY→mem.) at fixed commitment times can be determined. The resulting curves in Figure 5B are sigmoidal for all but the shortest commitment times, similar to the experimental insertion probabilities from which the biological hydrophobicity scale was determined.[4] Furthermore, the dependence of insertion probability on commitment time displays an asymptotic behavior, with the limiting case being near 50 s, which corresponds to the synthesis of 50 residues at a translation rate of 1 residue/s as assumed in the model. Although possibly coincidental, this number of residues agrees almost perfectly with the limiting case of 40−50 C-terminal residues seen experimentally.[30]

For each of the curves in Figure 5B, we calculated an apparent insertion free energy, which was defined identically to that in the biological hydrophobicity scale, i.e., $\Delta G_{app} = -kT \ln[p_{ins}(t)/p_{sec}(t)]$, where $p_{ins}(t)$ and $p_{sec}(t)$ are the probabilities of being membrane inserted or secreted at time t, respectively.

dx.doi.org/10.1021/ja310777k | J. Am. Chem. Soc. 2013, 135, 2291−2297

ΔG_{app} is plotted as a function of ΔG(SecY→mem.) for the different commitment times in Figure 5C. The relationship is almost exactly linear in all cases, with a slope of 0.65, indicating that the apparent insertion-free-energy scale, ΔG_{app}, is compressed with respect to the SecY-to-membrane transfer free energy. The latter free energy, ΔG(SecY→mem.), is already compressed with respect to the water-to-membrane transfer free energy,[8] suggesting that there are in fact two causes to explain the oft-cited compression of the biological hydrophobicity scale with respect to other scales.[6] Increasing the commitment time does not change the slope of a given line but does shift its intercept downward, thus decreasing the threshold for membrane insertion, as also observed experimentally.[16]

DISCUSSION

In this study, we have carried out a comprehensive exploration of a key stage of membrane protein development, the transfer of a TM segment from the translocon, here SecY, to the membrane. Simulations spanning nanoseconds to seconds permit a connection to be made between rapidly varying interactions of individual lipids, SecY, and the substrate helix on the one hand and the long-time-scale translocation and membrane-insertion processes on the other hand. Furthermore, PMF- and diffusion-based calculations elucidate the distinction between the actual free-energy differences for the helix in the channel and in the membrane and the apparent free energies measured experimentally.[5]

It was found that while the degree of opening of SecY's lateral gate has no apparent dependence on the hydrophobicity of the nascent chain inside the channel, at least on the 1−2-μs time scale simulated here, ribosome binding induces slight opening of the gate or prevents its closure. SecA-mediated translocation requires gate opening by at least 5 Å,[36] indicating that all parts of the nascent chain that enter SecY are at least transiently exposed to lipids. Our simulations of different nascent helices in SecY also indicate that, for a so-called closed gate, lipids can breach the gate to contact the helix, with the propensity to interact being directly related to helix hydrophobicity. For a hydrophobic TM segment, interaction with lipids draws it into the membrane, whereas a hydrophilic segment is driven back to the channel center to minimize its contact with lipids. Thus, direct lipid−protein interactions govern the short-time and short-distance behavior of a nascent polypeptide within the channel.

Translation and translocation, which occur on a much longer time scale than fluctuations of the nascent chain in the channel, were incorporated into a diffusion−elongation model for membrane insertion by imposing a time-dependent restriction (due to tethering of the helix in the SecY channel to the nascent chain in the ribosome exit tunnel) on diffusion of the TM segment out of the channel (see Figure 4). For the polyLeu and polyGln helices, the large change in free energy between channel and membrane makes their insertion (polyLeu) or lack thereof (polyGln) effectively absolute. However, the local free energy surface for the native SA is much flatter, generating a more varied time-dependent behavior than observed for the other two segments. Over typical translocation time scales, the SA partitions between channel and membrane-inserted states with a probability determined primarily by the local environment near the channel.

Extrapolation from the PMFs for the three tested helices to simplified, linear PMFs illustrates the full range of insertion probabilities and their dependence on ΔG between SecY and membrane. Variability of insertion probability was found to be greatest for values of ΔG(SecY→mem.) around 0, elucidating why the insertion of marginally hydrophobic helices is sensitive to multiple factors.[16,30] Derivation of the apparent insertion free energy, ΔG_{app}, i.e., the same as actually measured in the biological hydrophobicity scale, revealed a linear relationship between ΔG_{app} and the purely thermodynamic scale given by ΔG(SecY→mem.) (see Figure 5C). However, this relationship displays a compression of the biological scale relative to the thermodynamic one that is completely independent of the commitment time chosen, just as has been seen experimentally.[4,6] Taken together, our results suggest that the membrane-insertion process is not solely thermodynamic, but is rather a competition between kinetic and thermodynamic effects that mimics a two-state partitioning scheme under typical cellular and experimental conditions.

It is interesting to note that the compression of the scale observed here is due primarily to configurational entropy of the helical peptide in the membrane. The total area of membrane accessible to the nascent peptide increases with time and becomes rapidly much larger than the cross-section of the interior of the translocon. Unavoidably, this phenomenon shifts the apparent partition coefficient toward a membrane-inserted state. The effect of the growing configurational entropy, which always favors membrane insertion, can counteract unfavorable factors arising from the local molecular-based PMF. As a consequence, membrane insertion of slightly hydrophilic peptides, counterintuitively, arises to a significant degree.

The proposed mechanism for membrane insertion developed above is not intended to be taken as definitive or as complete. A particular deficiency is that movement from the channel to the lumen and backsliding are not explicitly accounted for in our description of the nascent chain. Thus, only trends, but not absolute probabilities of insertion, can be extracted from the model. Additionally, SecY was assumed to be constitutively open to the membrane, whereas the lateral gate has been shown to fluctuate, albeit on a time scale longer than that of the translation process.[31,36] Recent coarse-grained modeling of SecY function has also illustrated how membrane insertion can be both kinetically and thermodynamically determined, although the authors assumed, in contrast to our present finding, that lateral gate fluctuations are controlled by the TM segment's hydrophobicity.[12,51] Even if the lateral gate were constitutively open, membrane insertion can still be regulated by the translocon, provided that the continuity of the nascent chain keeps the TM segment near the channel. Neither model accounts for the retention of helices near the translocon due to protein−protein interactions with other channel partners,[50] which can prevent diffusion of the helix even with an extended C-terminal nascent chain in the cytoplasm. More extensive modeling and systematic experiments are needed to fully resolve the balance between thermodynamic and kinetic factors during insertion under a multitude of conditions, particularly in the case of multi-spanning membrane proteins.[52] Experiments probing the dependence of the biological hydrophobicity scale on kinetic factors, e.g., translation rate, would be especially illuminating.

ASSOCIATED CONTENT

Supporting Information

Detailed methods for the finite-element calculations, and additional figures and analysis. This material is available free of charge via the Internet at http://pubs.acs.org.

AUTHOR INFORMATION

Corresponding Author

roux@uchicago.edu; kschulte@ks.uiuc.edu

Notes

The authors declare no competing financial interest.

ACKNOWLEDGMENTS

This work was supported by grants from the National Institutes of Health (NIH, R01-GM067887, 9P41-GM104601 to K.S.) and the National Science Foundation (NSF, PHY-0822613 to K.S. and MCB-0920261 to B.R.). Simulations made use of the Extreme Science and Engineering Discovery Environment (XSEDE), which was supported by the NSF (OCI-1053575). Anton computer time was provided by the National Resource for Biomedical Supercomputing and the Pittsburgh Supercomputing Center through Grant RC2GM093307 from the NIH, using a machine donated by DE Shaw Research. J.C.G. is supported by a Director's Postdoctoral Fellowship from Argonne National Laboratory during completion of this work.

REFERENCES

(1) Park, E.; Rapoport, T. A. *Annu. Rev. Biophys.* **2012**, *41*, 21−40.
(2) Driessen, A. J. M.; Nouwen, N. *Annu. Rev. Biochem.* **2008**, *77*, 643−667.
(3) van den Berg, B.; Clemons, W. M., Jr.; Collinson, I.; Modis, Y.; Hartmann, E.; Harrison, S. C.; Rapoport, T. A. *Nature* **2004**, *427*, 36−44.
(4) Hessa, T.; Kim, H.; Bihlmaier, K.; Lundin, C.; Boekel, J.; Andersson, H.; Nilsson, I.; White, S. H.; von Heijne, G. *Nature* **2005**, *433*, 377−381.
(5) Hessa, T.; Meindl-Beinker, N. M.; Bernsel, A.; Kim, H.; Sato, Y.; Lerch-Bader, M.; Nilsson, I.; White, S. H.; von Heijne, G. *Nature* **2007**, *450*, 1026−1030.
(6) MacCallum, J. L.; Tieleman, D. P. *Trends Biochem. Sci.* **2011**, *36*, 653−662.
(7) Young, R.; Bremer, H. *Biochem. J.* **1976**, *160*, 185−194.
(8) Gumbart, J.; Chipot, C.; Schulten, K. *Proc. Natl. Acad. Sci. U.S.A.* **2011**, *108*, 3596−3601.
(9) White, S. H.; von Heijne, G. *Annu. Rev. Biophys.* **2008**, *37*, 23−42.
(10) Roux, B. *J. Gen. Physiol.* **2007**, *130*, 233−236.
(11) Gumbart, J.; Roux, B. *Biophys. J.* **2012**, *102*, 795−801.
(12) Zhang, B.; Miller, T. F. *Proc. Natl. Acad. Sci. U.S.A.* **2010**, *107*, 5399−5404.
(13) Zhang, B.; Miller, T. F. *J. Am. Chem. Soc.* **2012**, *134*, 13700−13707.
(14) Xie, K.; Hessa, T.; Seppälä, S.; Rapp, M.; von Heijne, G.; Dalbey, R. E. *Biochemistry* **2007**, *46*, 15153−15161.
(15) Botelho, S. C.; Österberg, M.; Reichert, A. S.; Yamano, K.; Björkholm, P.; Endo, T.; von Heijne, G.; Kim, H. *EMBO J.* **2011**, *30*, 1003−1011.
(16) Duong, F.; Wickner, W. *EMBO J.* **1998**, *17*, 696−705.
(17) Shaw, D. E.; et al. *Comm. ACM* **2008**, *51*, 91−97.
(18) Frauenfeld, J.; Gumbart, J.; van der Sluis, E. O.; Funes, S.; Gartmann, M.; Beatrix, B.; Mielke, T.; Berninghausen, O.; Becker, T.; Schulten, K.; Beckmann, R. *Nat. Struct. Mol. Biol.* **2011**, *18*, 614−621.
(19) Raetz, C. R.; Dowhan, W. *J. Biol. Chem.* **1990**, *265*, 1235−1238.
(20) Humphrey, W.; Dalke, A.; Schulten, K. *J. Mol. Graphics* **1996**, *14*, 33−38.
(21) Phillips, J. C.; Braun, R.; Wang, W.; Gumbart, J.; Tajkhorshid, E.; Villa, E.; Chipot, C.; Skeel, R. D.; Kale, L.; Schulten, K. *J. Comput. Chem.* **2005**, *26*, 1781−1802.
(22) MacKerell, A. D., Jr.; et al. *J. Phys. Chem. B* **1998**, *102*, 3586−3616.
(23) MacKerell, A. D., Jr.; Feig, M.; Brooks, C. L., III *J. Comput. Chem.* **2004**, *25*, 1400−1415.
(24) Klauda, J. B.; Venable, R. M.; Freites, J. A.; O'Connor, J. W.; Tobias, D. J.; Mondragon-Ramirez, C.; Vorobyov, I.; MacKerell, A. D., Jr.; Pastor, R. W. *J. Phys. Chem. B* **2010**, *114*, 7830−7843.
(25) Ulmschneider, J. P.; Smith, J. C.; White, S. H.; Ulmschneider, M. B. *J. Am. Chem. Soc.* **2011**, *133*, 15487−15495.
(26) Torrie, G. M.; Valleau, J. P. *J. Comput. Phys* **1977**, *23*, 187−199.
(27) Roux, B. *Comput. Phys. Commun.* **1995**, *91*, 275−282.
(28) Hénin, J.; Forin, G.; Chipot, C.; Klein, M. L. *J. Chem. Theory Comput.* **2010**, *6*, 35−47.
(29) Kumar, S.; Bouzida, D.; Swendsen, R. H.; Kollman, P. A.; Rosenberg, J. M. *J. Comput. Chem.* **1992**, *13*, 1011−1021.
(30) Hessa, T.; Monné, M.; von Heijne, G. *EMBO Rep.* **2003**, *4*, 178−183.
(31) Cheng, Z.; Gilmore, R. *Nat. Struct. Mol. Biol.* **2006**, *13*, 930−936.
(32) Henin, J.; Tajkhorshid, E.; Schulten, K.; Chipot, C. *Biophys. J.* **2008**, *94*, 832−839.
(33) Frey, S.; Tamm, L. K. *Biochem. J.* **1990**, *272*, 713−719.
(34) Goder, V.; Crottet, P.; Spiess, M. *EMBO J.* **2000**, *19*, 6704−6712.
(35) Monné, M.; Hessa, T.; Thissen, L.; von Heijne, G. *FEBS Lett.* **2005**, *272*, 28−36.
(36) du Plessis, D. J. F.; Berrelkamp, G.; Nouwen, N.; Driessen, A. J. M. *J. Biol. Chem.* **2009**, *284*, 15805−15814.
(37) Tsukazaki, T.; Mori, H.; Fukai, S.; Ishitani, R.; Mori, T.; Dohmae, N.; Perederina, A.; Sugita, Y.; Vassylyev, D. G.; Ito, K.; Nureki, O. *Nature* **2008**, *455*, 988−991.
(38) Zimmer, J.; Nam, Y.; Rapoport, T. A. *Nature* **2008**, *455*, 936−943.
(39) Egea, P. F.; Stroud, R. M. *Proc. Natl. Acad. Sci. U.S.A.* **2010**, *40*, 17182−17187.
(40) Simon, S.; Blobel, G. *Cell* **1991**, *65*, 371−380.
(41) Heritage, D.; Wonderlin, W. F. *J. Biol. Chem.* **2001**, *276*, 22655−22662.
(42) Wonderlin, W. F. *Pflug. Arch. Eur. J. Physiol.* **2009**, *457*, 917−930.
(43) Gumbart, J.; Trabuco, L. G.; Schreiner, E.; Villa, E.; Schulten, K. *Structure* **2009**, *17*, 1453−1464.
(44) Gumbart, J.; Schulten, K. *J. Gen. Physiol.* **2008**, *132*, 709−719.
(45) Hessa, T.; White, S. H.; von Heijne, G. *Science* **2005**, *307*, 1427.
(46) Bol, R.; de Wit, J. G.; Driessen, A. J. M. *J. Biol. Chem.* **2007**, *282*, 29785−29793.
(47) Gumbart, J.; Chipot, C.; Schulten, K. *J. Am. Chem. Soc.* **2011**, *133*, 7602−7607.
(48) Wang, Y.; Markwick, P. R. L.; de Oliveira, C. A. F.; McCammon, J. A. *J. Chem. Theory Comput.* **2011**, *7*, 3199−3207.
(49) Ismail, N.; Hedman, R.; Schiller, N.; von Heijne, G. *Nat. Struct. Mol. Biol.* **2012**, *19*, 1018−1023.
(50) Hou, B.; Lin, P.-J.; Johnson, A. E. *Mol. Cell* **2012**, *48*, 398−408.
(51) Zhang, B.; Miller, T. F. *Cell Rep.* **2012**, *2*, 927−937.
(52) Rychkova, A.; Vicatos, S.; Warshel, A. *Proc. Natl. Acad. Sci. U.S.A.* **2010**, *107*, 17598−17603.